Front. Phys. 11(6), 113202 (2016)
DOI 10.1007/s11467-016-0593-2

RESEARCH ARTICLE

Subcycle electron emission in sequential double ionization by elliptical laser pulses

Ai-Hong Tong (童爱红)[1,†], Ying-Bin Li (李盈傧)[2]

[1] *Department of Physics and Mechanical & Electrical Engineering, Hubei University of Education, Wuhan 430205, China*
[2] *National Laboratory of Solid State Microstructures and Department of Physics, Nanjing University, Nanjing 210093, China*
Corresponding author. E-mail: [†]tongah@hue.edu.cn
Received March 1, 2016; accepted May 10, 2016

Using a classical ensemble method, we have investigated sequential double ionization (SDI) of Ar atoms driven by elliptical laser pulses. The results show that the ion momentum distribution of the Ar atoms depends strongly on the pulse duration. As the pulse duration increases, the ion momentum distribution changes from two bands to four bands and then to six bands and finally to an eight-band structure. Back analysis of double ionization trajectories shows that the variation of the band structure originates from pulse duration dependent multiple ionization bursts of the second electron. Our calculations indicate that the subcycle electron emission in the SDI could be more easily accessed by using elliptical laser pulses with a longer wavelength. Moreover, we show that there is good correspondence between the scaled radial momentum and the ionization time.

Keywords sequential double ionization, pulse duration, elliptical laser pulse, subcycle electron emission

PACS numbers 32.80.Rm, 32.80.Fb, 34.50.Fa

1 Introduction

Double ionization (DI) has been a hot topic in strong-field physics during the last decades. According to the character of the DI process, there are two different DI routes: nonsequential double ionization (NSDI) [1–11] and sequential double ionization (SDI) [12–17]. In NSDI, the second electron is ionized by the recollision of the first ionized electron with the parent nucleus [18, 19]. Because of the recollision, the two electrons in NSDI exhibit a strong correlated behavior. In SDI, the two electrons are emitted sequentially by the laser field. Usually, SDI dominates in either linear laser fields with a high enough intensity or in elliptical laser fields. The SDI process is relatively simpler than the NSDI. However, SDI by elliptically polarized laser pulses can provide considerable ionization information that is unavailable in NSDI, e.g., the release time of the electrons [12, 20, 21].

In recent years, SDI in elliptical laser fields has attracted increasing attention and revealed some new interesting phenomena. In Ref. [13, 14], the two electrons from SDI show a strong angular correlation. In Ref. [15], the measured electron momentum distributions display a conflict with the prediction of the independent electron model, where the ratio of the parallel to antiparallel emissions of the SDI events shows an oscillating behavior as a function of the laser intensity. In Ref. [16], the measured release time of the first electron agrees well with the prediction of the independent electron model, while that of the second electron is much earlier than the prediction of the independent electron model; the measured doubly charged ion momentum distributions depend on the laser intensity, such that they evolve from a three-band structure to a four-band structure with the increase of the laser intensity. The classical ensemble method has excellently reproduced these experimental results and intuitively shown the sequential nature of double ionization [17, 20]. Classical calculations also show that the ion momentum spectrum for multiple ionization will exhibit more bands. For example, it was predicted that the ion momentum spectrum for sequential triple ionization will exhibit eight bands [21]. This prediction has been observed in a very recent experiment, where the ion momentum spectra for the triple ionization of Ne^+ show a six-band structure [22]. From these structures, the sat-

uration ionization intensity and the ionization time for each ionization step are successfully extracted [22].

In SDI generated by the elliptically polarized laser field, the ionization of each electron usually lasts longer than one optical cycle and there is one ionization burst during each half cycle. Therefore, there will be multiple ionization bursts for each electron. However, the subcycle ionization bursts of SDI have not been observed in previous experiments. This may be because the wavelength of the laser pulse in previous experiments is about 800 nm, where the subcycle ionization bursts could not be resolved. In this paper, we theoretically investigate SDI by elliptical laser fields with longer wavelengths. Our calculations predict that, depending on the pulse duration, the ion momentum spectra of a doubly charged ion exhibit different numbers of bands. With the pulse duration increasing, the spectrum evolves from a two-band structure into a four-band structure, then a six-band structure, and finally into an eight-band structure. Our analysis shows that these phenomena are the manifestation of the subcycle ionization bursts of the second electron for both short pulses and long pulses and that of the first electron only for long pulses. Our calculations indicate that the subcycle electron emission in SDI can be more easily observed by choosing elliptical laser pulses with longer wavelengths.

2 Theoretical model

In the classical model of two- or multi-electron systems with the coulomb potential for the ion-electron interaction, the atoms suffer autoionization and are unstable. This problem can be solved by employing the classical model with a soft-core potential [23–29]. In the past decade, the soft-core potential classical model (SPCM) [26–29] has achieved great success in exploring the correlated electron dynamics in NSDI, where the crucial ionization process is insensitive to the second ionization potential. However, the SPCM is deficient in describing strong-field SDI. This is because the SPCM cannot match the first and second ionization potentials with those of the investigated target, yet the ionization probability of both electrons depends sensitively on the ionization potential. This deficiency can be avoided by the Heisenberg-core potential that can not only prevent autoionization but also give ground-configuration energies of the multielectron atoms [17, 20]. This potential has been extensively employed to classically investigate atomic and molecular collisions [30–33], and strong-field ionization [34, 35]. Here, we employ this model to study SDI by elliptical laser fields with different pulse durations. Its accurate description of SDI has been previously confirmed [17, 20].

In the Heisenberg-core potential classical model (HPCM), the evolution of the two-electron system is determined by the equations (atomic units are used throughout this paper unless stated otherwise):

$$\frac{\mathrm{d}r_i}{\mathrm{d}t}=\frac{\partial H}{\partial p_i},\quad \frac{\mathrm{d}p_i}{\mathrm{d}t}=-\frac{\partial H}{\partial r_i}, \tag{1}$$

where H is the Hamiltonian of the two-electron system in the presence of the laser field and is expressed as

$$H=\frac{1}{|\boldsymbol{r}_1-\boldsymbol{r}_2|}+\sum_{i=1,2}\left[-\frac{2}{r_i}+\frac{p_i^2}{2}+V_H(r_i,p_i)\right] +(\boldsymbol{r}_1+\boldsymbol{r}_2)\cdot\boldsymbol{E}, \tag{2}$$

where r_i, p_i are the position and canonical momentum of the i_{th} electron, respectively. $\boldsymbol{E}(t)$ is a circularly polarized electric field, which is given as

$$\boldsymbol{E}(t)=f(t)\left[\frac{1}{\sqrt{\varepsilon^2+1}}\cos(\omega t+\varphi)\hat{x}+\frac{\varepsilon}{\sqrt{\varepsilon^2+1}}\sin(\omega t+\varphi)\hat{y}\right], \tag{3}$$

where $f(t)=E_0\sin^2\left(\frac{\pi t}{NT}\right)$ is the field envelope, and ω, $\varepsilon, \varphi, E_0, T, N$ are frequency, ellipticity, carrier-envelope phase (CEP), amplitude, period, and period number of the laser pulse, respectively. $V_H(r_i,p_i)$ is the Heisenberg-core potential, which is expressed as $V_H(r_i,p_i)=\xi^2/(4\alpha r_i^2)\exp\{\alpha[1-(r_ip_i/\xi)^4]\}$. The parameter α indicates the rigidity of the Heisenberg core. For Ar, the rigidity parameter α is set to 2, then the parameter ξ is chosen to match the second ionization potential of Ar (-1.01 a.u.) and ξ is set to 1.225 [17].

The ground-state energy of Ar is set to the sum of the first and second ionization potentials (-1.59 a.u.) and the initial distributions of the ground-state atom in phase space are obtained with the approach in the SPCM [26–29].

Once the initial state is obtained, the laser is turned on. The evolution of the two-electron system follows Eq. (1) above. In our calculations, the laser intensity is 6×10^{15} W/cm^2, the wavelength is 1600 nm, the ellipticity is 0.75, and N ranges from 4 to 14.

At the end of the laser pulse, we examine the energy of the electrons. We define that the electron is ionized if its final energy becomes positive for the first time. Double ionization is defined when both electrons possess positive energies at the end of the pulse. The energy of the electron is composed of kinetic energy, electron-ion interaction energy, Heisenberg-core potential energy, and half of the electron-electron interaction energy. In our calculations, all of the DI events are SDI since recollisions are completely suppressed because of the large elliptical laser pulse employed in our calculations.

3 Results and discussion

Figure 1 displays the ion momentum distributions in the polarization plane for the SDI of Ar by elliptically polarized laser pulses with different pulse durations, where N is the period number ranging from 4 to 14. The ion momentum of Ar^{2+} is obtained by the negative sum of the two electron momentum vectors because the momentum of the absorbed photons is negligibly small, i.e., $p_{x,\mathrm{ion}} = -(p_{x,e1} + p_{x,e2})$. In these calculations, CEP is random for each atom, corresponding to a phase-unlocked experiment. Figure 1 shows that the ion momentum distributions in the direction of the minor elliptical axis ($\hat{y}$ axis) exhibit a band structure and the number of the bands strongly depends on the laser duration. For the pulse duration $N = 4$, the distribution shows two bands. When the pulse duration increases to $N = 6$, two more bands appear even though they are relatively weaker. For $N = 8$, the outer two bands become more obvious. Moreover, two more bands between the inner and the outer bands appear, displaying a six-band structure. This six-band structure is also very clear at $N = 10$ and 12. However, with the pulse duration increasing further, the two inner bands gradually disappear and almost vanish for the case of $N = 14$. Meanwhile, one can find that the fourth pair of bands (marked as B_4) start to appear, showing the eight-band structure in Fig. 1(f).

This change of ion momentum distributions with pulse duration can be more clearly seen in Fig. 2, where the distributions of Fig. 1 are integrated over the $p_{x,\mathrm{ion}}$ axis. Figure 2 shows the ion momentum distributions in the direction of the minor elliptical axis ($\hat{y}$ axis). For the pulse duration $N = 4$, the spectrum exhibits two sharp inner peaks, which are labeled as P_1. There are also two flat outer peaks (P_2) whose corresponding bands in Fig. 1(a) are not obvious. As the pulse duration increases, the two outer peaks (P_2) become stronger at $N = 6$. For the case of $N = 8$, two P_2 peaks are even stronger and two more peaks (P_3), between P_1 and P_2, appear. The spectrum exhibits a very clear six-peak structure [Fig. 2(c)]. As the pulse duration increases further, the peaks P_1 become gradually weaker. Finally, the P_1 peaks almost disappear at $N = 14$. Meanwhile, two more peaks (P_4) start to appear for $N = 14$ [Fig. 2(f)]. Additionally, one can see that the separation between the two P_1 peaks decreases when the pulse duration increases.

In order to understand the physical process for the dependence of the ion momentum distributions on pulse duration, we fix CEP at $\varphi = 0$ and recalculate the SDI with the same elliptical laser pulse as in Fig. 1. The ion momentum distributions in the polarization plane are shown in Fig. 3. Seen in Fig. 3, the ion momentum distributions also show a band structure and the number of bands also depends sensitively on the pulse duration. However, the distributions are asymmetric for short pulses, which is due to the asymmetry of the electric field of the short pulses. For example, at the pulse duration $N = 4$, only one band with negative momentum

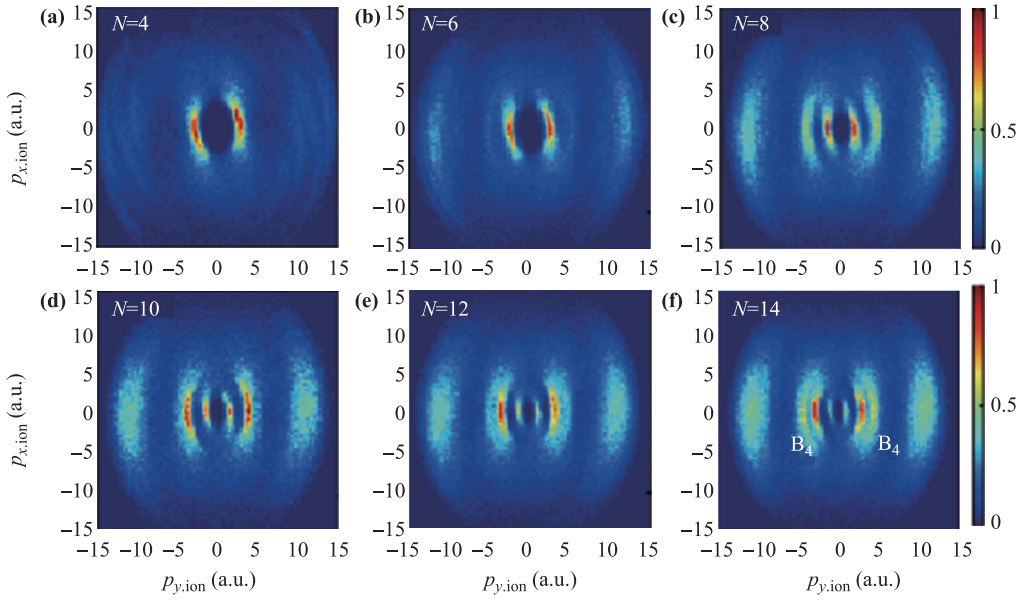

Fig. 1 Ion momentum distributions in the laser polarization plane for different pulse durations. The ellipticity of the laser pulses is 0.75, the intensity is 6.0 PW/cm^2, and the wavelength is 1600 nm. The CEP is randomly chosen for each trajectory. The ensembles are 400 000.

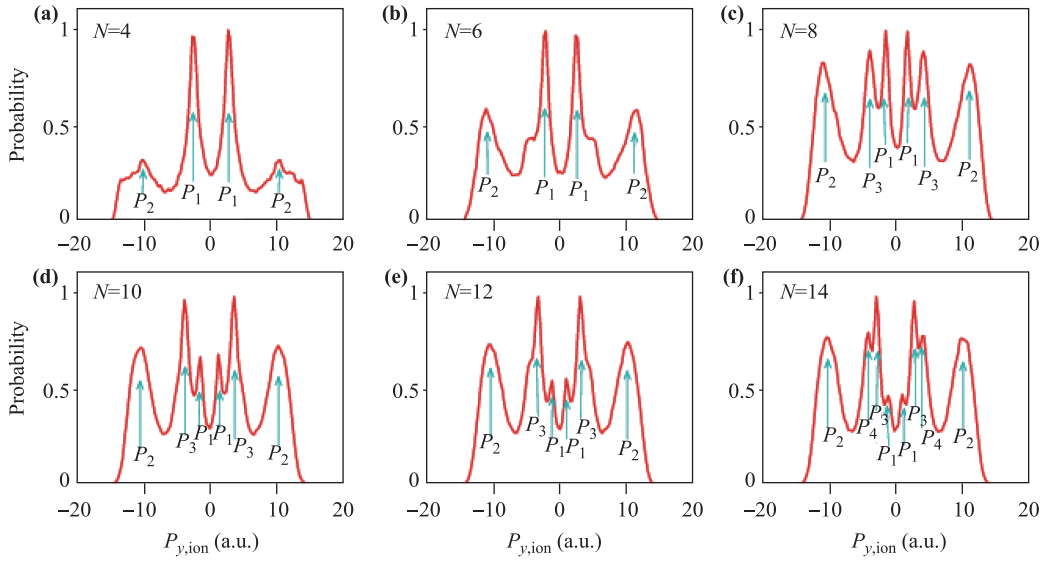

Fig. 2 Ion momentum distributions along the minor elliptical axis ($\hat{y}$ axis) for different pulse durations. The laser parameters are the same as those in Fig. 1.

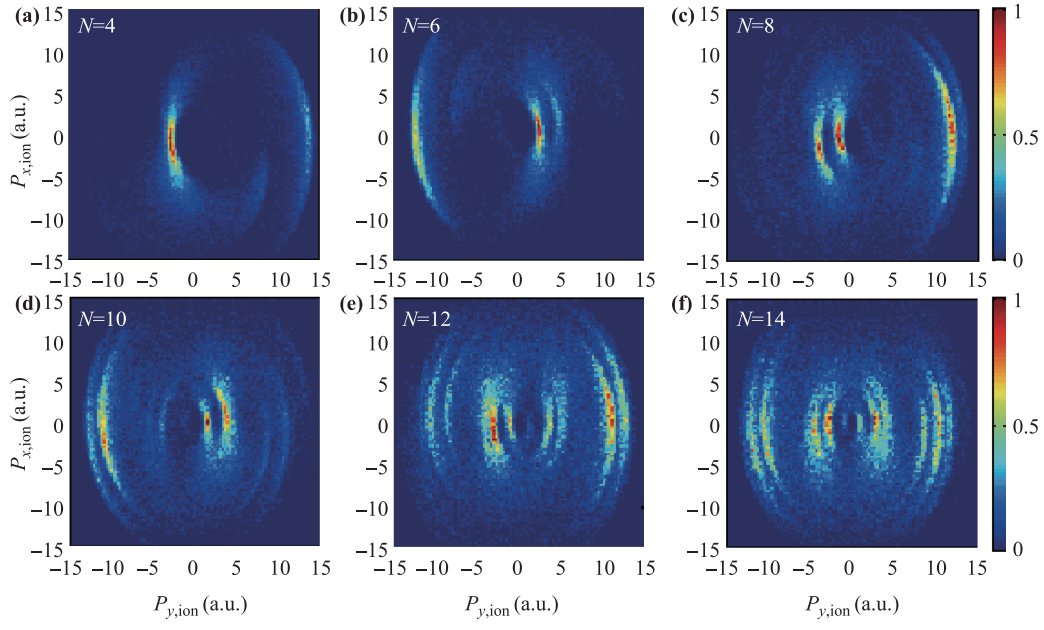

Fig. 3 Ion momentum distributions in the laser polarization plane for different pulse durations with $\varphi = 0$. Other parameters are the same as those in Fig. 1.

appears and the band with positive momentum is absent. The absent band will appear for other CEPs. This is the same situation for pulse durations up to $N = 10$. For longer pulses, the distributions become gradually symmetric.

The results above show that the ion momentum distributions in the polarization plane for the SDI of Ar by elliptically polarized laser pulses depend strongly on the pulse duration of the laser pulses. As we know, the ion momentum is a good reflection of the ionization dynamics of the electrons. In order to explain the origin of the above pulse duration dependence of ion momentum distributions, we trace the history of the two electron trajectories and find the ionization times of the two electrons. The ionization time of the first electron is defined as the instant when the energy of one electron is positive for the first time, while the ionization time of the second electron is the instant when both electrons have positive

energies.

Figure 4 shows the distribution of the first ionization time (t_{i1}) versus the second ionization time (t_{i2}) for $N = 4, 8, 10$, and 14. For the pulse duration $N = 4$, the ionization time distribution is clustered in two regions, which are labeled "1" and "2". When pulse duration increases, a third clustering region "3" and fourth clustering region "4" start to appear in turn at $N = 8$ and $N = 10$. For even larger pulse durations, more concentrations appear. For example, the clustering region "5" is obviously distributed at $N = 14$ [Fig. 4(d)]. Additionally seen in Fig. 4, for short pulse durations ($N = 4$ to $N = 10$), there is only one ionization burst for the first electrons, meaning that the first electron is completely ionized within a half cycle at this high laser intensity. For the long pulse $N = 14$, there are two ionization bursts for the first electron. For the second electron, there are two to many ionization bursts. These distributions directly show subcycle electron bursts of the second electron for both short pulses and long pulses, and that of the first electron only for long pulses. By projecting these clustering regions to the t_{i1} axis and t_{i2} axis, one can find that the delay time between t_{i2} and t_{i1} is integer multiples of the half cycle. In Fig. 4, the marks "1", "2", "3", "4", and "5" are also used to represent the regions with a delay time ($t_{i2} - t_{i1}$) of one, two, three, four, and five times of the half cycle, respectively. Furthermore, the population in region "1" decreases as the pulse duration increases.

Since the initial momentum at ionization is negligible, the final momenta of the electrons are $p_{ei} = A(t_i) = -\int_{t_i}^{+\infty} E(t)dt$, where t_i is the ionization time of the i_{th} electron and $E(t)$ is the electric field. As a result, the direction of the final momentum of an electron is perpendicular to the electric field at the instant of ionization. Seen from Fig. 4, both electrons are emitted around the field extrema of the major elliptical direction, thus, the electrons are emitted in the minor elliptical direction. When their ionization time delay is even (odd) multiples of the half cycle, the two electrons will emit in the same (opposite) directions. For the events with ionization time distributed in the regions "2" and "4" in Fig. 4, the two electrons emit in the same direction and the corresponding ion momentum distribution is located at peaks P_2 of Fig. 2. For the concentrations "1", "3" and "5" in Fig. 4, the two electrons emit in opposite directions, and result in the inner peaks P_1, P_3 and P_4 of Fig. 2, respectively.

Based on the above relation between the ionization time and the ion momentum, the evolution of the ion momentum distribution with pulse duration can be easily explained as follows. For $N = 4$, the ionization time distribution has a strong concentration in region "1" and a weak concentration in region "2", so the ion momentum distribution notably dominates at peaks P_1 [Fig. 2(a)]. When the pulse duration increases to $N = 8$, region "3" emerges in the ionization time distribution, corresponding to the appearance of the ion momentum peaks P_3 in Fig. 2 (c). For $N = 10$, DI events related to the ionization time concentration "4" also contribute to the outer ion momentum peaks P_2. As the pulse duration increases to $N = 14$, the emergence of region "5" lead to the appearance of peaks P_4 in Fig. 2(d). Since the population of the ionization time in region "1" gradually decreases, peaks P_1 become gradually weaker, and almost disappear at $N = 14$. Thus, the multiple band structure in the ion momentum distributions comes from the subcycle electron bursts.

Next, we analyze the reason for the decrease of the separation of the two P_1 peaks with an increasing pulse duration. The separation of the two P_1 peaks is determined by the momentum difference of the two electrons. For this pair of peaks, the ionization time delay between the two electrons is a half cycle. For a fixed laser intensity, the momentum difference decreases as the pulse duration increases. Consequently, the separation of the two P_1 peaks decreases with an increasing pulse duration [Fig. 2].

It has been demonstrated that the radial momentum is an injective function of the ionization time with the condition that the electrons are ionized before the peak of the pulses [17]. Here, we clearly display the relation-

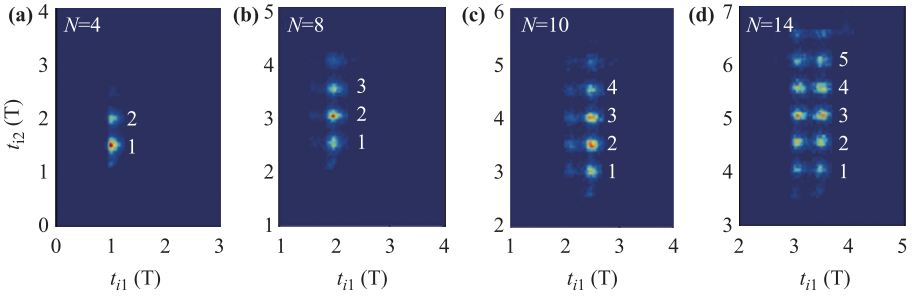

Fig. 4 Time distributions between the first ionization time (t_{i1}) and the second ionization time (t_{i2}) for different pulse duration with CEP $\varphi = 0$.

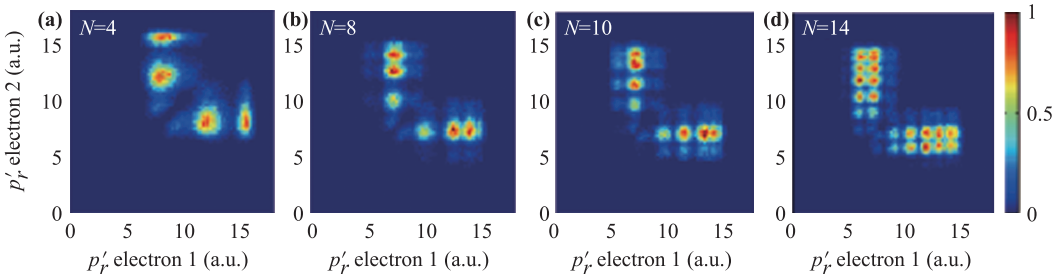

Fig. 5 The electron correlation spectra for the scaled radial momentum with CEP $\varphi = 0$.

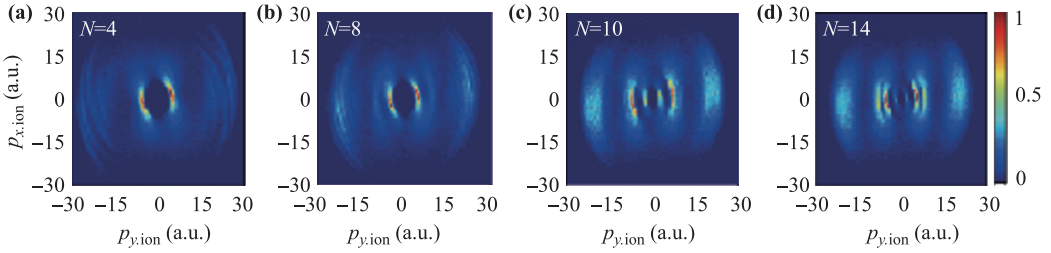

Fig. 6 Ion momentum distributions in the laser polarization plane for different pulse durations with $\lambda = 3000$ nm. Other parameters are the same as those in Fig. 1.

ship between the scaled radial electron momentums with ionization time. In Fig. 5, we display the electron correlation spectra for the scaled radial momentum p'_r for $N = 4, 8, 10$, and 14, where p'_r is defined as

$$p'_{r,i} = \sqrt{(\varepsilon^2+1)p_{x,i}^2 + [(\varepsilon^2+1)/\varepsilon^2]p_{y,i}^2}, \tag{4}$$

where $i = 1, 2$ is the electron label. These spectra are symmetric with respect to the diagonal because we do not distinguish the first and the second electrons here. For the high laser intensity in our calculations, both electrons are ionized within the rising edge of the laser pulse, and thus the earlier ionized electrons will achieve a smaller final momentum. Therefore, we can distinguish which electron is ionized first based on the final momentums. In the following, we denote the electron with the smaller final momentum (thus ionized first) as the first electron and the other electron as the second electron. As shown in Fig. 5, for short pulse durations ($N = 4$ to $N = 10$), there is only one concentration of scaled radial momentum for the first electron. However, for the second electron, the concentrations of the scaled radial momentum depend on the pulse duration. For $N = 4, 8$, and 10, the number of the concentrations are 2, 3, and 4, respectively. For long pulses $N = 14$, there are two concentrations of scaled radial momentum for the first electron and many concentrations for the second electron. Comparing Fig. 5 with Fig. 4, it is easy to build a good correspondence between the scaled radial moment and the ionization time.

We further calculate the SDI of the Ar atoms driven by the same elliptical laser pulses except that the wavelength is even longer (3000 nm). The ion momentum distributions in the polarization plane for $N = 4, 6, 10$, and 14 are displayed in Fig. 6. Seen in Fig. 6, the influence of the pulse duration on the ion momentum distributions in the minor direction is same as the case in Fig. 1. However, in the multiple band structure, it is more obvious that the separation between the bands is larger, which will be favorable for the observation of the subcycle multiple ionization bursts in experiments.

4 Conclusion

In conclusion, using the HPCM, we investigated the SDI of Ar by an elliptical laser pulse. We resolved the multiple-band structure in the ion momentum spectra. This structure originates from the multiple ionization bursts of the second electrons and directly reveals the subcycle electron emission nature of the SDI in the elliptical laser field. Our calculations confirm that longer wavelengths will be more favorable for the observation of these subcycle multiple ionization bursts. Moreover, our results display a good correspondence between the scaled radial electron momentum and the ionization time.

Acknowledgements This work was supported by the National Natural Science Foundation of China under Grant No. 11404105.

References

1. Th. Weber, H. Giessen, M. Weckenbrock, G. Urbasch, A. Staudte, L. Spielberger, O. Jagutzki, V. Mergel, M. Vollmer, and R. Dörner, Correlated electron emission in multiphoton double ionization, *Nature* 405, 658 (2000)
2. Y. Liu, S. Tschuch, A. Rudenko, M. Dürr, M. Siegel, U. Morgner, R. Moshammer, and J. Ullrich, Strong-field double ionization of Ar below the recollision threshold, *Phys. Rev. Lett.* 101(5), 053001 (2008)
3. M. Weckenbrock, D. Zeidler, A. Staudte, T. Weber, M. Schöffler, M. Meckel, S. Kammer, M. Smolarski, O. Jagutzki, V. R. Bhardwaj, D. M. Rayner, D. M. Villeneuve, P. B. Corkum, and R. Dörner, Full differential rates for femtosecond multiphoton double ionization of neon, *Phys. Rev. Lett.* 92(21), 213002 (2004)
4. J. Liu, D. Ye, J. Chen, and X. Liu, Complex dynamics of correlated electrons in molecular double ionization by an ultrashort intense laser pulse, *Phys. Rev. Lett.* 99(1), 013003 (2007)
5. Y. Zhou, C. Huang, A. Tong, Q. Liao, and P. Lu, Correlated electron dynamics in nonsequential double ionization by orthogonal two-color laser pulses, *Opt. Express* 19(3), 2301 (2011)
6. L. Fu, G. Xin, D. Ye, and J. Liu, Recollision dynamics and phase diagram for nonsequential double ionization with circularly polarized laser fields, *Phys. Rev. Lett.* 108(10), 103601 (2012)
7. J. Chen and C. H. Nam, Ion momentum distributions for He single and double ionization in strong laser fields, *Phys. Rev. A* 66(5), 053415 (2000)
8. A. Staudte, C. Ruiz, M. Schöffler, S. Schössler, D. Zeidler, Th. Weber, M. Meckel, D. M. Villeneuve, P. B. Corkum, A. Becker, and R. Dörner, Binary and recoil collisions in strong field double ionization of helium, *Phys. Rev. Lett.* 99(26), 263002 (2007)
9. M. Wu, Y. Wang, X. Liu, W. D. Li, X. L. Hao, and J. Chen, Coulomb-potential effects in nonsequential double ionization under elliptical polarization, *Phys. Rev. A* 87(1), 013431 (2013)
10. A. Tong, Ion momentum analysis of double ionization of stretched molecules by circularly polarized laser pulses, *Opt. Commun.* 312, 252 (2014)
11. X. Ma, Y. Zhou, and P. Lu, Multiple recollisions in strong-field nonsequential double ionization, *Phys. Rev. A* 93(1), 013425 (2016)
12. C. M. Maharjan, A. S. Alnaser, X. Tong, B. Ulrich, P. Ranitovic, S. Ghimire, Z. Chang, I. V. Litvinyuk, and C. L. Cocke, Momentum imaging of doubly charged ions of Ne and Ar in the sequential ionization region, *Phys. Rev. A* 72(4), 041403(R) (2005)
13. A. Fleischer, H. J. Wörner, L. Arissian, L. R. Liu, M. Meckel, A. Rippert, R. Dörner, D. M. Villeneuve, P. B. Corkum, and A. Staudte, Probing angular correlations in sequential double ionization, *Phys. Rev. Lett.* 107(11), 113003 (2011)
14. X. Wang, J. Tian, and J. H. Eberly, Angular correlation in strong-field double ionization under circular polarization, *Phys. Rev. Lett.* 110(7), 073001 (2013)
15. A. N. Pfeiffer, C. Cirelli, M. Smolarski, X. Wang, J. H. Eberly, R. Dörner, and U. Keller, Breakdown of the independent electron approximation in sequential double ionization, *New J. Phys.* 13(9), 093008 (2011)
16. A. N. Pfeiffer, C. Cirelli, M. Smolarski, R. Dörner, and U. Keller, Timing the release in sequential double ionization, *Nat. Phys.* 7(5), 428 (2011)
17. Y. Zhou, C. Huang, Q. Liao, and P. Lu, Classical simulations including electron correlations for sequential double ionization, *Phys. Rev. Lett.* 109(5), 053004 (2012)
18. P. B. Corkum, Plasma perspective on strong field multiphoton ionization, *Phys. Rev. Lett.* 71(13), 1994 (1993)
19. Y. Zhou, O. I. Tolstikhin, and T. Morishita, Near-forward rescattering photoelectron holography in strong-field ionization: extraction of the phase of the scattering amplitude, *Phys. Rev. Lett.* 116(17), 173001 (2016)
20. Y. Zhou, Q. Zhang, C. Huang, and P. Lu, Classical description of strong-field double ionization by elliptical laser pulses, *Phys. Rev. A* 86(4), 043427 (2012)
21. X. Wang and J. H. Eberly, Classical theory of high-field atomic ionization using elliptical polarization, *Phys. Rev. A* 86(1), 013421 (2012)
22. P. Wustelt, M. Möller, T. Rathje, A. M. Sayler, T. Stöhlker, and G. G. Paulus, Momentum-resolved study of the saturation intensity in multiple ionization, *Phys. Rev. A* 91(3), 031401 (2015)
23. J. Javanainen, J. H. Eberly, and Q. Su, Numerical simulations of multiphoton ionization and above-threshold electron spectra, *Phys. Rev. A* 38(7), 3430 (1988)
24. Q. Su and J. H. Eberly, Model atom for multiphoton physics, *Phys. Rev. A* 44(9), 5997 (1991)
25. X. Wang and J. H. Eberly, Effect of elliptical polarization on strong-field short-pulse double ionization, *Phys. Rev. Lett.* 103(10), 103007 (2009)
26. S. L. Haan, L. Breen, A. Karim, and J. H. Eberly, Variable time lag and backward ejection in full-dimensional analysis of strong-field double ionization, *Phys. Rev. Lett.* 97(10), 103008 (2006)
27. Y. Zhou, C. Huang, Q. Liao, W. Hong, and P. Lu, Control the revisit time of the electron wave packet, *Opt. Lett.* 36(15), 2758 (2011)
28. P. J. Ho, R. Panfili, S. L. Haan, and J. H. Eberly, Nonsequential double ionization as a completely classical photoelectric effect, *Phys. Rev. Lett.* 94(9), 093002 (2005)
29. A. Tong, D. Liu, and G. Feng, Nonsequential double ionization of diatomic molecules by elliptically polarized laser pulses, *Chin. Phys. B* 23(10), 103302 (2014)
30. D. Zajfman and D. Maor, Heisenberg core in classical-trajectory Monto Carlo calculations of ionization and charge exchange, *Phys. Rev. Lett.* 56(4), 320 (1986)
31. J. S. Cohen, Quasiclassical-trajectory Monte Carlo methods for collisions with two-electron atoms, *Phys. Rev. A* 54(1), 573 (1996)

32. W. A. Beck and L. Wilets, Semiclassical description of proton stopping by atomic and molecular targets, *Phys. Rev. A* 55(4), 2821 (1997)

33. P. B. Lerner, K. J. LaGattuta, and J. S. Cohen, Ionization of helium by a short pulse of radiation: A Fermi molecular-dynamics calculation, *Phys. Rev. A* 49(1), R12 (1994)

34. E. Lötstedt, T. Kato, and K. Yamanouchi, Classical dynamics of laser-driven D_3^+, *Phys. Rev. Lett.* 106(20), 203001 (2011)

35. Y. Zhou, C. Huang, and P. Lu, Revealing the multi-electron effects in sequential double ionization using classical simulations, *Opt. Express* 20(18), 20201 (2012)